

## Revisiting the photodissociation dynamics of the phenyl radical

Neil C. Cole-Filipiak, Mark Shapero, Bogdan Negru, and Daniel M. Neumark

Citation: *The Journal of Chemical Physics* **141**, 104307 (2014); doi: 10.1063/1.4894398

View online: <http://dx.doi.org/10.1063/1.4894398>

View Table of Contents: <http://scitation.aip.org/content/aip/journal/jcp/141/10?ver=pdfcov>

Published by the [AIP Publishing](#)

---

### Articles you may be interested in

[O\(3PJ\) formation and desorption by 157-nm photoirradiation of amorphous solid water](#)

*J. Chem. Phys.* **140**, 094702 (2014); 10.1063/1.4867194

[Photodissociation dynamics of the phenyl radical via photofragment translational spectroscopy](#)

*J. Chem. Phys.* **133**, 074302 (2010); 10.1063/1.3473743

[Photodissociation of the propargyl and propynyl \( C 3 D 3 \) radicals at 248 and 193 nm](#)

*J. Chem. Phys.* **130**, 044310 (2009); 10.1063/1.3067705

[Photofragment translational spectroscopy of propargyl radicals at 248 nm](#)

*J. Chem. Phys.* **128**, 114303 (2008); 10.1063/1.2840350

[D atom loss in the photodissociation of the DNCN radical: Implications for prompt NO formation](#)

*J. Chem. Phys.* **126**, 114311 (2007); 10.1063/1.2710271

---

An advertisement for the COMSOL Conference 2014 Boston. The background is a vibrant blue with a complex, multi-colored pattern of concentric, swirling lines in shades of yellow, orange, and red, resembling a stylized atom or a simulation. On the left, the text 'COMSOL CONFERENCE 2014 BOSTON' is written in white, sans-serif font. In the center, the main headline 'The Multiphysics Simulation Event of the Year' is displayed in a large, white, sans-serif font. On the right side, there is a white rectangular button with the text 'LEARN MORE >>' in blue. At the bottom right corner, the COMSOL logo is visible, consisting of a small square icon followed by the word 'COMSOL' in white.

## Revisiting the photodissociation dynamics of the phenyl radical

Neil C. Cole-Filipiak, Mark Shapero, Bogdan Negru,<sup>a)</sup> and Daniel M. Neumark<sup>b)</sup>

*Department of Chemistry, University of California, Berkeley, California 94720, USA and Chemical Sciences Division, Lawrence Berkeley National Laboratory, Berkeley, California 94720, USA*

(Received 27 June 2014; accepted 19 August 2014; published online 9 September 2014)

We have reinvestigated the photodissociation dynamics of the phenyl radical at 248 nm and 193 nm *via* photofragment translational spectroscopy under a variety of experimental conditions aimed at reducing the nascent internal energy of the phenyl radical and eliminating signal from contaminants. Under these optimized conditions, slower translational energy ( $P(E_T)$ ) distributions for H-atom loss were seen at both wavelengths than in previously reported work. At 193 nm, the branching ratio for  $C_2H_2$  loss *vs.* H-atom loss was found to be  $0.2 \pm 0.1$ , a significantly lower value than was obtained previously in our laboratory. The new branching ratio agrees with calculated Rice-Ramsperger-Kassel-Marcus rate constants, suggesting that the photodissociation of the phenyl radical at 193 nm can be treated using statistical models. The effects of experimental conditions on the  $P(E_T)$  distributions and product branching ratios are discussed. © 2014 AIP Publishing LLC. [<http://dx.doi.org/10.1063/1.4894398>]

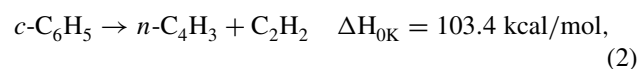
### I. INTRODUCTION

The phenyl radical,  $c\text{-C}_6\text{H}_5$ , is a key intermediate in the combustion of aromatic hydrocarbons<sup>1</sup> and formation of polycyclic aromatic hydrocarbons (PAH).<sup>1–3</sup> The role of the phenyl radical in soot<sup>4,5</sup> formation has been of particular interest, as soot particles, which can be formed from PAH,<sup>6,7</sup> have been implicated in both health and environmental issues.<sup>8,9</sup> The phenyl radical has also been implicated in the chemistry of the interstellar medium, particularly in the formation of PAH.<sup>10–12</sup> In this work, we focus on the unimolecular chemistry of the phenyl radical by re-investigating its ultraviolet photodissociation at excitation wavelengths of 248 nm and 193 nm, with particular emphasis on product branching at 193 nm.

The spectroscopy of the phenyl radical is fairly well characterized. Several of its electronic properties have been measured, including its ultraviolet absorption spectrum,<sup>13,14</sup> ionization potential,<sup>15,16</sup> photoionization cross section,<sup>17</sup> and electron affinity.<sup>18</sup> The electronic states and vibronic spectra of the phenyl radical have also been calculated.<sup>19</sup> The  $1^2B_1 \leftarrow \tilde{X}^2A_1$  transition of the phenyl radical was recently studied using cavity ring-down spectroscopy.<sup>20</sup> Rotationally resolved infrared spectra have been measured<sup>21,22</sup> and investigated theoretically.<sup>23</sup>

The reactions of the phenyl radical are also of considerable interest. Early theoretical work focused on its ring-opening and subsequent dissociation or bimolecular cyclization.<sup>24–27</sup> From the ring-opened structure, two dissociation pathways can occur: C–H bond cleavage to form  $l\text{-C}_6\text{H}_4 + \text{H}$  and C–C bond cleavage to form  $C_2H_2 + C_4H_3$ . Madden *et al.*<sup>28</sup> calculated a ground state potential energy surface (PES), shown in Fig. 1, along with Rice-Ramsperger-

Kassel-Marcus (RRKM) rate constants for the phenyl radical that demonstrated the importance of C–H bond cleavage from the cyclic species to form *o*-benzynes + H,<sup>28</sup> the lowest energy product channel. The energetics for these three channels, based on calculations by Mebel and Landera,<sup>29</sup> are as follows:



Later work by Olivella and Solé<sup>30</sup> focused on the ring opening and cyclization pathways of the phenyl radical. A small exit barrier ( $\sim 4$  kcal/mol)<sup>27</sup> for channel 1 that was not present in the PES from Madden *et al.*<sup>28</sup> has been reported by several groups.<sup>31,39</sup> Wang *et al.*<sup>31</sup> further explored the RRKM rate constants for the direct H-atom loss channel at higher temperatures than the previous work.<sup>28</sup> The PES was later expanded upon<sup>27,32,33</sup> to include an additional acetylene loss channel and a  $C_4H_4 + C_2H$  channel.<sup>34</sup>

Early experimental work identified the role of the phenyl radical in combustion subsequent to the thermolysis of aromatic molecules such as benzene,<sup>35–38</sup> thereby stimulating interest in the reactions of the phenyl radical itself. Kinetics of reactions with the phenyl radical have been performed in the liquid phase,<sup>39,40</sup> and several gas phase bimolecular kinetics and dynamics experiments have been carried out, most notably by the Lin<sup>41–43</sup> and Kaiser<sup>10,11</sup> groups. The photodissociation of benzene<sup>44</sup> and nitrosobenzene<sup>45</sup> have been shown to produce vibrationally excited phenyl radicals, which then spontaneously decay to form a hydrogen atom and a  $C_6H_4$  fragment. These studies concluded that *o*-benzynes was the most likely  $C_6H_4$  fragment. Recent investigations of the reactions of the phenyl radical have included the crossed molecular beam study of phenyl with propene and *trans*-2-butene<sup>46</sup>

<sup>a)</sup>Present address: Department of Chemistry, Northwestern University, 2145 Sheridan Rd., Evanston, Illinois 60208, USA.

<sup>b)</sup>Author to whom correspondence should be addressed. Electronic mail: dneumark@berkeley.edu.

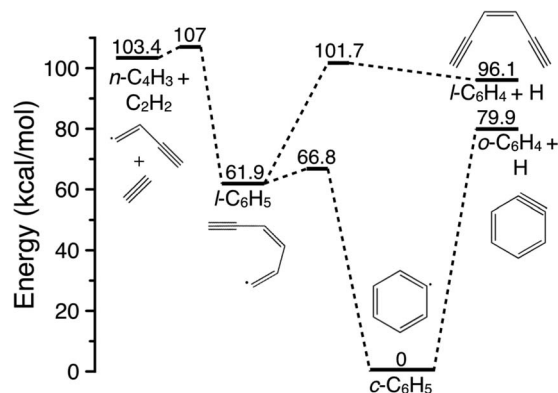


FIG. 1. Simplified ground state potential energy diagram of the phenyl radical showing the three primary dissociation pathways. Energies are from Ref. 29, structures are from Refs. 28 and 29.

as well as several further experimental and computational studies by Kaiser and co-workers.<sup>12,47–49</sup>

In work from our laboratory, Negru *et al.*<sup>50</sup> investigated the photodissociation of the phenyl radical at 248 and 193 nm *via* photofragment translational spectroscopy. The radicals were produced by flash pyrolysis<sup>51</sup> of nitrosobenzene ( $C_6H_5NO$ ). At 248 nm, the phenyl radical was found to dissociate to  $C_6H_4 + H$  and the resulting translational energy distribution suggested that dissociation occurred *via* channel 1, a result consistent with the PES and RRKM rate constants of Madden *et al.*<sup>28</sup> At 193 nm, both H-atom and acetylene loss pathways were observed. Signal from channels 1 and 3 could not be distinguished and was thus referred to as “combined H-atom loss.” Translational energy distributions for both product channels suggested statistical ground state dissociation dynamics. However, the product branching ratio between acetylene loss and the combined H-atom loss channel was determined to be 5.3 in favor of acetylene loss, a somewhat surprising result given that channel 2 is higher in energy than channels 1 and 3. Using the PES and vibrational frequencies of Lin and co-workers,<sup>28</sup> we were unable to reproduce the experimental branching ratio with RRKM rate constants and speculated that the lower energy  $i-C_4H_3 + C_2H_2$  channel<sup>27</sup> would allow for more product flux into acetylene loss. As RRKM rate constants were unavailable for this channel, this proposal was not tested.

Our investigation was followed by a study of phenyl radical photodissociation by Song *et al.*<sup>52</sup> *via* H-atom time-of-flight using resonance enhanced multiphoton ionization. In the wavelength range of 215 nm to 268 nm, their translational energy distributions were consistent with ground state dissociation dynamics. The distributions also indicated that either only channel 1 was accessed or that both channels 1 and 3 were accessed but the channel 3 contribution was small, a conclusion supported by the available RRKM rate constants.<sup>28,52</sup> As only H-atoms are detected using this technique, Song *et al.*<sup>52</sup> were unable to investigate the acetylene loss channel.

Motivated by the results of Negru *et al.*,<sup>50</sup> recent theoretical work by Mebel and Landera<sup>29</sup> examined a larger number of channels for phenyl radical dissociation. Detailed RRKM calculations at a variety of energies were also carried out in

an effort to characterize the relative importance of each product channel, finding that the three channels originally investigated by Madden *et al.*<sup>28</sup> to be of greatest importance over a wide range of excitation energies. Dissociation *via* the  $i-C_4H_3 + C_2H_2$  channel was found to be insignificant, owing to a substantial isomerization barrier along the reaction coordinate to form these products. Mebel and Landera were unable to reproduce the experimental branching ratio with their calculated surface and the absorption of only one 193 nm photon (148 kcal/mol): their calculated channel 2 to channels (1 + 3) branching ratio was 0.17, favoring the combined H-atom loss channel. Significantly, they found that channel 2 becomes dominant at higher excitation energies, *e.g.*, 182 kcal/mol corresponding to absorption by one photon at 157 nm. In a final effort to explain the experimental results, they calculated several conical intersections between the first excited and ground electronic states, two of which would place substantial vibrational energy into the acetylene loss coordinate, and suggested that these conical intersections might result in non-statistical dynamics that could explain the experimental results of Negru *et al.* However, no excited state dynamics calculations were performed, so the importance of these conical intersections could not be quantified.

In an effort to reconcile the experimental and theoretical results, we have reinvestigated the photodissociation of the phenyl radical at 193 nm and 248 nm using photofragment translational spectroscopy. Results were obtained under a variety of different experimental conditions aimed at reducing the radical internal energy. We find that a minor modification of source conditions, using 10%  $N_2$  in He for the carrier gas instead of pure He, yields noticeably slower translational energy distributions for H-atom loss at 193 nm and 248 nm. Under these conditions, and taking steps to insure that all the nitrosobenzene precursor molecules were pyrolyzed in our radical source, we find a  $C_2H_2$  loss vs. H-atom loss branching ratio at 193 nm of  $0.2 \pm 0.1$ , largely in agreement with statistical theoretical results.<sup>29</sup> Our results will be discussed in light of previous work, particularly the results from Negru *et al.*

## II. EXPERIMENTAL

Phenyl radical photodissociation was studied on a modified crossed molecular beam machine using a fixed source and rotating time-of-flight (TOF) detector with electron impact (EI) ionization and a quadrupole mass filter. Details of this apparatus have been described previously.<sup>50,53–55</sup> As in our previous investigation,<sup>50</sup> phenyl radicals were produced *via* flash pyrolysis of nitrosobenzene (Sigma,  $\geq 97\%$ ) using a resistively heated SiC pyrolysis source based on the design by Kohn *et al.*<sup>51</sup> The source was recently modified to include additional water cooling lines on the pulsed valve assembly and an aluminum heat shield around the SiC tube and electrodes, resulting in a significant increase in source stability and thus allowing for increased TOF integration times. A gas mixture of 1.6 atm of  $\sim 10\%$   $N_2$  in He was flowed over a room temperature sample of nitrosobenzene, resulting in a nitrosobenzene concentration of  $\sim 0.5\%$ , and was introduced into vacuum by expansion through a piezoelectric pulsed valve with the pyrolysis source attached.<sup>56</sup>

The resulting phenyl radical beam was skimmed and collimated by two skimmers that isolate the source from the scattering chamber. The collimated molecular beam was crossed at  $90^\circ$  with the  $1 \times 3 \text{ mm}^2$  focused output of a GAM EX100/500 excimer laser operating at either 193 nm with typical pulse energies of 4 mJ, or 248 nm with typical pulse energies of 12 mJ; corresponding fluences were 133 and  $400 \text{ mJ cm}^{-2}$ . The fluence at 193 nm was considerably lower than the  $500 \text{ mJ cm}^{-2}$  used by Negru *et al.*<sup>50</sup> The pulsed valve and laser were operated at 200 and 100 Hz, respectively, in order to perform background subtraction. Scattered photofragments were detected as a function of laboratory angle  $\Theta_{\text{lab}}$  in the plane defined by the laser and molecular beams. After entering the detector, photofragments were ionized *via* EI ionization, mass-selected with a quadrupole mass filter, and ultimately detected with a Daly-style ion detector.<sup>57</sup> Ion counts as a function of time relative to the laser pulse were recorded with a multichannel scaler interfaced to a computer and the resulting TOF spectra were acquired for  $10^5$ – $10^6$  laser shots at each laboratory angle. TOF spectra were simulated using an iterative forward convolution method to determine the center-of-mass translational energy distributions.

The molecular beam was characterized using a spinning, slotted chopper disk. Typical beam velocities were  $\sim 1700 \text{ m/s}$  with speed ratios of 4–5. The beam was further characterized by monitoring the nitrosobenzene signal ( $m/z = 107$ ) and phenyl radical signal ( $m/z = 77$ ) while the pyrolysis source was incrementally heated until the nitrosobenzene signal was fully depleted. Incomplete depletion of the precursor may have been a possible source of error in our previous work,<sup>50</sup> as discussed in Sec. V. Any remaining signal at  $m/z = 77$  was attributed to the phenyl radical, an assumption tested in Sec. III. For comparison to our previous investigation, the experiments were also repeated with 1.6 atm of pure He. Under these conditions, typical beam velocities were  $\sim 2500 \text{ m/s}$  with speed ratios of 6–7, similar to the beam characteristics described by Negru *et al.*<sup>50</sup>

Further experiments aimed at testing the effect of carrier gas composition were carried out using 1.6 atm of 10% Ar in He or 10%  $\text{CO}_2$  in He, again directly applied to both the sample and pulsed valve. These source conditions resulted in beam velocities  $\sim 200 \text{ m/s}$  slower than the  $\text{N}_2/\text{He}$  mixture but had otherwise similar beam characteristics.

### III. RESULTS

TOF spectra were taken at multiple angles for  $m/z = 76$  ( $\text{C}_6\text{H}_4^+$ ),  $m/z = 51$  ( $\text{C}_4\text{H}_3^+$ ), and  $m/z = 26$  ( $\text{C}_2\text{H}_2^+$ ), representing parent ions of photoproducts from channels 1–3, and for  $m/z = 50$  ( $\text{C}_4\text{H}_2^+$ ), a possible daughter ion from all three channels resulting from dissociative ionization in the EI ionizer. At 248 nm, spectra taken at  $m/z = 76$  for  $\Theta_{\text{lab}} = 3^\circ$ – $7^\circ$  were found to have one feature; no signal was observed in spectra taken at larger scattering angles. Representative spectra are shown in Figs. 2(a) and 2(b). The data are shown as open circles while the solid line is from a forward convolution simulation of a translational energy distribution (see Sec. IV). No other photoproducts were observed, and all spectra at  $m/z \leq 76$  appeared to be from dissociative ionization of

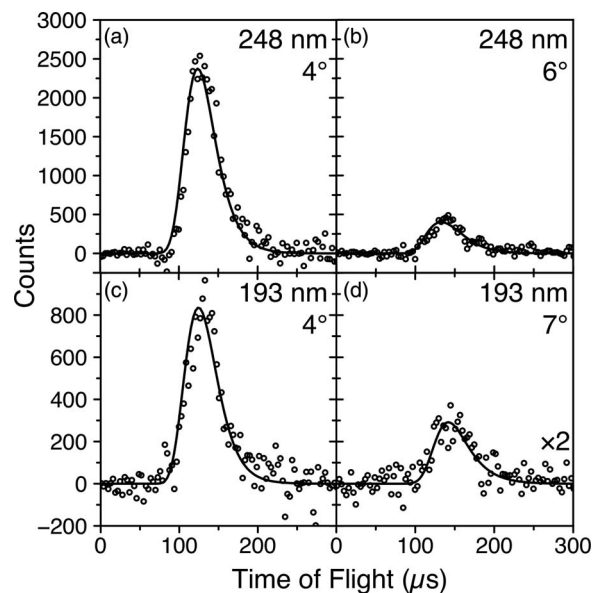


FIG. 2. Representative  $m/z = 76$  TOF spectra taken in the  $\text{N}_2/\text{He}$  carrier gas mixture at 248 nm, (a) and (b), or 193 nm, (c) and (d). The data are shown as open circles while the solid line shows the simulation from either the 248 nm  $P(E_T)$  distribution in Fig. 7 or the 193 nm  $P(E_T)$  distribution in Fig. 8. The number of laser shots is 300 000 and 500 000 for panels (a) and (b), respectively; and 200 000 and 400 000 for panels (c) and (d), respectively.

the  $\text{C}_6\text{H}_4$  photofragment. As in our previous work,<sup>50</sup> all of the signal at 248 nm is attributed to channel 1.

At 193 nm, spectra at  $m/z = 76$  were observed for  $\Theta_{\text{lab}} = 3^\circ$ – $9^\circ$  and representative TOF spectra are shown in Figs. 2(c) and 2(d). These spectra are attributed to channels 1 and 3. TOF spectra for H-atoms at  $m/z = 1$  were not recorded due to unfavorable kinematics and high background levels. Figure 3 shows representative TOF spectra for  $m/z = 51$  and  $m/z = 26$ . These spectra are assigned to the  $\text{C}_4\text{H}_3$  and  $\text{C}_2\text{H}_2$  photofragments from phenyl radical dissociation *via* channel 2.

Sample TOF spectra for  $m/z = 50$  and  $\Theta_{\text{lab}} < 10^\circ$  at 193 nm are shown in Figure 4. These spectra show two features, attributed to the dissociative ionization of the  $\text{C}_6\text{H}_4$  and  $\text{C}_4\text{H}_3$  photofragments and can be used to determine the product branching ratio. Compared to our previous work in pure He,<sup>50</sup> the two features are better-resolved because the molecular beam velocity is slower using the 10%  $\text{N}_2$  in He carrier gas mixture. Details of all channel assignments and the product branching ratio will be discussed in Sec. IV.

Similar  $m/z = 76$  and  $m/z = 50$  TOF spectra to those shown in Figures 2 and 4 were taken with the current experimental conditions using a pure He carrier gas. Figure 5 shows representative results for  $m/z = 76$  and compares them to forward convolutions from two translational energy distributions (Sec. IV). Experiments with the Ar/He and  $\text{CO}_2/\text{He}$  carrier gas mixtures resulted in TOF spectra similar to those shown in Figures 2 and 3; sample 193 nm Ar/He spectra are shown and discussed in the supplementary material.<sup>56</sup>

### IV. ANALYSIS

The results presented in Sec. III suggest that phenyl radical photodissociation at 193 nm occurs *via* two main

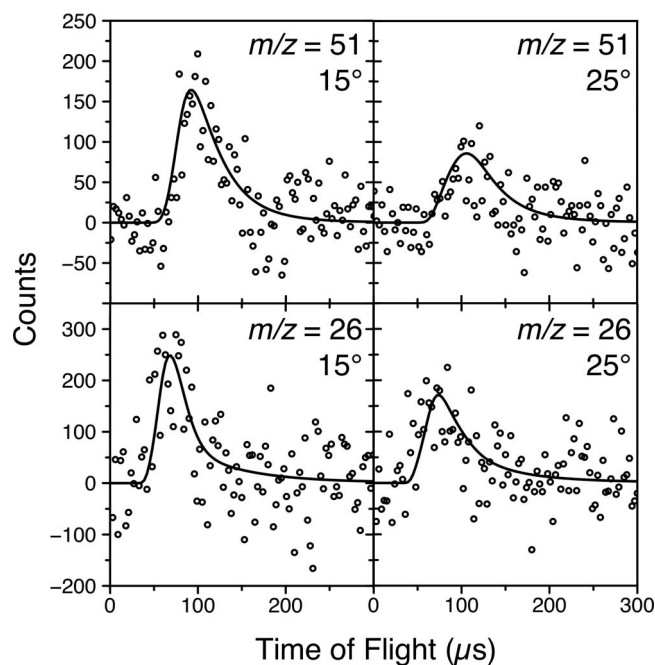


FIG. 3. Sample TOF spectra taken at  $m/z = 51$  (top row) and  $m/z = 26$  (bottom row) in the  $\text{N}_2/\text{He}$  carrier gas mixture and 193 nm photoexcitation. The data are shown as open circles while the solid line shows the simulation from the  $P(E_T)$  in Fig. 9. All spectra were simultaneously simulated with a single  $P(E_T)$  distribution. All spectra shown were averaged for  $10^6$  laser shots.

pathways—an apparent C–C bond fission pathway and an H-atom loss channel—while only H-atom loss appears at 248 nm. These assignments are consistent with the kinematics of phenyl radical dissociation after excitation from one photon, as illustrated by the Newton diagram in Fig. 6 where the circles represent the maximum center-of-mass frame velocity for each specified photofragment after photodissociation at 193 nm. The  $\text{C}_6\text{H}_4$  products from channels 1 and 3 are confined to a very small angular range while photofragments from channel 2 are scattered over a larger angular range with scattering of the acetylene fragment unconstrained to a maximum  $\Theta_{\text{lab}}$ . TOF spectra at  $m/z = 76$  were not observed beyond  $9^\circ$  at 193 nm or  $7^\circ$  at 248 nm, supporting their assignment to a phenyl radical H-atom loss pathway. Signals at  $m/z = 51$  and  $m/z = 26$  were observed outside of the maximum laboratory angle for the  $\text{C}_6\text{H}_4$  fragments, eliminating the pos-

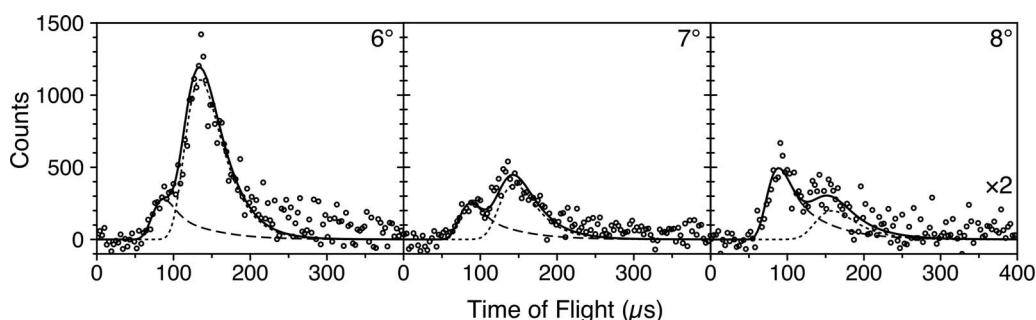


FIG. 4. Representative  $m/z = 50$  TOF spectra taken at  $\Theta_{\text{lab}} = 6^\circ$ – $8^\circ$  in  $\text{N}_2/\text{He}$  carrier gas mixture and 193 nm photoexcitation. Data are shown as open circles. The fast feature (dashed line) is simulated by the channel 2  $P(E_T)$  shown in Fig. 9 while the slow feature (dotted line) is simulated by the channel (1 + 3)  $P(E_T)$  shown in Fig. 8. The solid line is the total TOF simulation. The number of laser shots is 500 000 for the  $6^\circ$  and  $7^\circ$  TOF spectra and 400 000 for the  $8^\circ$  TOF spectrum.

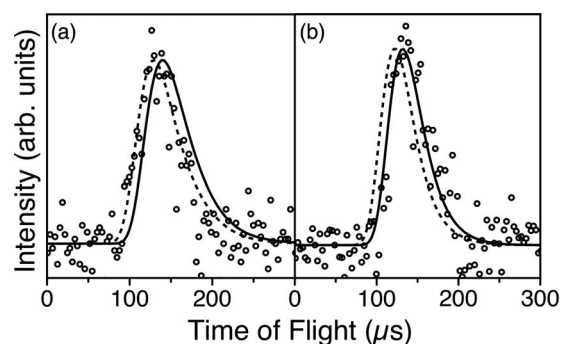


FIG. 5. (a) TOF spectrum (open circles) of  $m/z = 76$  and  $6^\circ$  at 193 nm in He with simulations from  $\text{N}_2/\text{He}$  (solid line) and pure He (dotted line)  $P(E_T)$  distributions shown in Fig. 8. (b) An equivalent spectrum taken with the  $\text{N}_2/\text{He}$  carrier gas mixture at  $m/z = 76$  and  $6^\circ$ .

sibility that these spectra are due to dissociative ionization of the  $m/z = 76$  photofragment and supporting their assignment to channel 2. This assignment can be confirmed by determining if the TOF spectra for the two fragments are “momentum-matched,” as discussed below.

To analyze these results quantitatively, center-of-mass photofragment translational energy and angular distributions,  $P(E_T, \Theta)$ , were generated for each channel by simulating the observed TOF spectra. These  $P(E_T, \Theta)$  distributions can then be rewritten as uncoupled center-of-mass translational energy distributions  $P(E_T)$  and angular distributions  $I(\Theta, E_T)$ ,

$$P(E_T, \Theta) = P(E_T)I(\Theta, E_T). \quad (4)$$

To simulate the TOF spectra, assumed  $P(E_T)$  and  $I(\Theta, E_T)$  distributions were used with the PHOTRAN forward convolution program.<sup>58</sup> The  $P(E_T)$  distribution was then adjusted point-wise until satisfactory agreement between the TOF data and the simulation for that channel was achieved. While an anisotropic angular distribution is possible, satisfactory agreement between spectral data and the simulations was achieved assuming isotropic distributions for all center-of-mass translational energies  $E_T$ .

By conservation of energy,  $E_T$  is given by

$$E_T = h\nu - D_0 + E_0 + E_{\text{int}}, \quad (5)$$

where  $h\nu$  is the photon energy,  $D_0$  is the bond dissociation energy for a given channel,  $E_0$  is the nascent internal energy

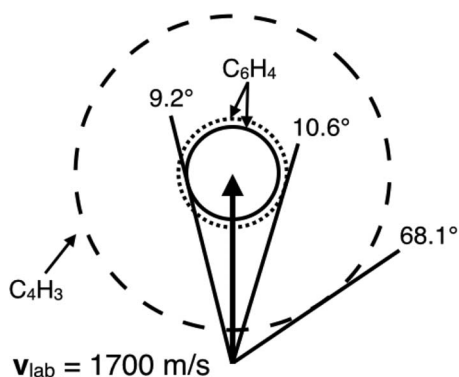


FIG. 6. Newton diagram for the phenyl radical dissociation at 193 nm under the current experimental conditions. Each circle represents the maximum center-of-mass velocity for a photofragment based on Eqs. (1)–(3) and (5). The dotted circle corresponds to the heavy fragment of channel 1, the dashed circle to the heavy fragment of channel 2, and the solid circle corresponds to the heavy fragment of channel 3. Maximum scattering angles are shown.

of the phenyl radicals, and  $E_{\text{int}}$  is the total internal energy of the resulting photofragments. In the limit of cold radicals ( $E_0 = 0$ ), each channel's maximum translational energy is  $E_{\text{avail}}$ , given by  $h\nu - D_0$ , and is used to generate the Newton diagram in Fig. 6.

Figure 7 shows the  $P(E_T)$  distribution for H-atom loss *via* channel 1 at 248 nm used to simulate the observed TOF feature in Figures 2(a) and 2(b). The assignment of these features to channel 1 is substantiated by the result that there appear to be no other phenyl radical photodissociation products at 248 nm. The TOF simulations for H-atom loss at 193 nm, shown as a solid line in Figures 2(c) and 2(d), were generated by the  $P(E_T)$  distribution shown as a black line in Fig. 8. As in our previous investigation,<sup>50</sup> we were unable to distinguish between channels 1 and 3, since most of the signal occurs below  $E_{\text{avail}}$  for both channels. Thus, this  $P(E_T)$  distribution represents the combined channels (1 + 3). While the probability of translational energies greater than 30 kcal/mol is quite small (see Fig. 8 inset), a trial  $P(E_T)$  distribution with zero probability at these energies resulted in noticeably poorer agreement between simulations and experimental data. As  $m/z = 76$  TOF data were not acquired for  $\Theta_{\text{lab}} < 3^\circ$ , energies below 5 kcal/mol are uncertain. Adjustments to the 3 kcal/mol point, however, still had an effect on the TOF simulations and the current placement was found to produce the best agreement with experimental data. The probability at  $E_T = 0$  kcal/mol was assumed to be zero based on previous work<sup>50,52</sup> and functional forms for translational energy distributions.<sup>59</sup>

TOF spectra at  $m/z = 76$  taken in pure He carrier gas are not simulated by the  $P(E_T)$  distribution used to fit the  $\text{N}_2/\text{He}$  data, as can be seen in Fig. 5(a), but these data are well-simulated by the somewhat faster distribution given in Figure 8 (dark gray line). This  $P(E_T)$  distribution is slower than our previously published distribution at 193 nm,<sup>50</sup> but has a higher probability than the  $\text{N}_2/\text{He}$  distribution for all  $E_T > 6$  kcal/mol. The panel in Fig. 5(b) shows that this faster distribution does not simulate the  $\text{N}_2/\text{He}$  data. TOF spectra taken using Ar/He and  $\text{CO}_2/\text{He}$  mixes, on the other hand, were fit well using the distribution that simulated the  $\text{N}_2/\text{He}$  data.

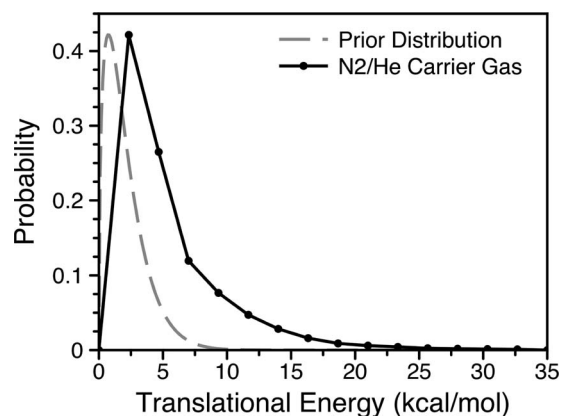


FIG. 7. Translational energy distribution for channel 1 at 248 nm. Due to the minimum experimental scattering angle of  $3^\circ$ , energies below 6 kcal/mol are less certain than higher translational energies. Characteristics of this distribution are given in Table I. The dashed, gray line shows the prior distribution for this channel as discussed in Sec. IV.

Hence, the  $P(E_T)$  distribution for H atom loss clearly depends on whether a pure He or mixed carrier gas is used, but does not depend noticeably on which gas is mixed with the He.

The  $P(E_T)$  distribution for channel 2 is shown in Fig. 9 and the respective TOF simulations are overlaid on Fig. 3. Refinements to the distribution were made by simulating spectra at  $m/z = 50$  and  $\Theta_{\text{lab}} > 10^\circ$ , where there is no contribution from channels 1 or 3, as the signal at  $m/z = 50$  is substantially higher than at either  $m/z = 51$  or  $m/z = 26$ . The result that both the  $m/z = 51$  and  $m/z = 26$  TOF spectra are simulated by the same  $P(E_T)$  distribution indicates that these fragments are momentum-matched, which supports the conclusions that the spectra in Fig. 3 are the result of acetylene loss from the phenyl radical.

Characteristics of all  $P(E_T)$  distributions are given in Table I. At 193 nm, the average translational energy  $\langle E_T \rangle$  for H-atom loss in the  $\text{N}_2/\text{He}$  mixture is 4 kcal/mol below that for pure He. In fact, it is slower than our previously

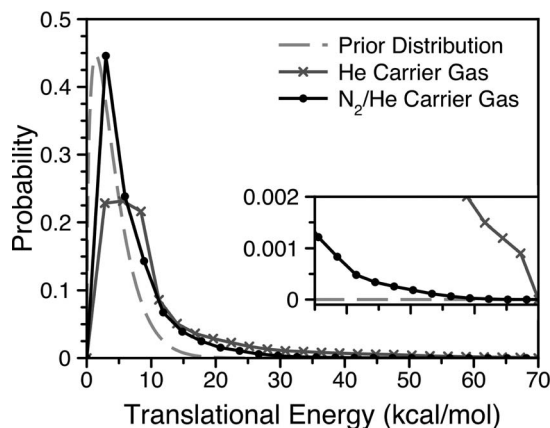


FIG. 8. Translational energy distribution for the combined H-atom loss channel at 193 nm for the  $\text{N}_2/\text{He}$  (black line) and pure He (dark gray line) carrier gases. Due to the minimum scattering angle of  $3^\circ$ , energies below 5 kcal/mol are less certain than higher translational energies. The probability from 35 kcal/mol to 80 kcal/mol for the  $\text{N}_2/\text{He}$  distribution is shown in the inset. Characteristics of these distributions are given in Table I. The dashed, gray line shows the prior distribution as discussed in Sec. IV.

TABLE I. Characteristics of the  $P(E_T)$  distributions derived in this work: available energy  $E_{\text{avail}}$ , the maximum translational energy of the distribution  $E_{T,\text{max}}$ , the average translational energy  $\langle E_T \rangle$ , and the average fraction of  $E_{\text{avail}}$  partitioned into translational energy  $\langle f_T \rangle$ . Wavelengths are given in nm and energy values are in kcal/mol.

Channel	Wavelength	Carrier gas	Figure	$E_{\text{avail}}$	$E_{T,\text{max}}$	$\langle E_T \rangle$	$\langle f_T \rangle$
1	248	N <sub>2</sub> /He	6	35	35	6	0.17
(1 + 3)	193	N <sub>2</sub> /He	7, black line	68	65	7	0.10
(1 + 3)	193	He	7, dark gray line	68	70	11	0.16
(1 + 3)	193	He	Fig. 9 of Ref. 50	68	66	16	0.24
2	193	N <sub>2</sub> /He	8	46	46	13	0.28

published  $P(E_T)$  for H-atom loss at 248 nm.<sup>50</sup> While  $\langle E_T \rangle$  for channel 2 has not changed, the  $P(E_T)$  distribution in Fig. 9 does have higher probability at the peak translational energy and slightly decreased probability above 25 kcal/mol compared to our previous distribution.<sup>50</sup> At 248 nm, the  $P(E_T)$  distribution for H-atom loss is also slower than previously published distributions.<sup>50,52</sup> Although our experiment does not distinguish between channels 1 and 3 at 193 nm, it is of interest to note from Table I that the  $\langle f_T \rangle = \langle E_T \rangle / E_{\text{avail}}$  for H-atom loss is smaller at 193 nm than 248 nm. Such a result could occur if there were significant channel 3 production at 193 nm, since the available energy for this channel is 16 kcal/mol lower than for channel 1.

For comparison to experiment, prior distributions for the H-atom loss  $P(E_T)$  distributions at 248 nm and 193 nm were calculated. The prior distribution has the functional form<sup>59</sup>

$$P(E_T | E_{\text{avail}}) \propto E_T^{1/2} \rho_{\text{vr}}(E_{\text{avail}} - E_T), \quad (6)$$

where  $E_T$  is the translational energy of the photofragment,  $E_{\text{avail}}$  is the available energy given by  $h\nu - D_0$  in Eq. (5), and  $\rho_{\text{vr}}(E_{\text{avail}} - E_T)$  is the total rotational-vibrational density of states for the pair of fragments. All vibrational degrees of freedom were treated as classical harmonic oscillators, i.e.,  $\rho_{\text{v}} \propto E^{\text{s-1}}$ , and  $E_{\text{avail}}$  was calculated for channel 1. The resulting prior distributions for H-atom loss at 193 nm and 248 nm are shown as dashed, light gray lines in Figures 7 and 8. These distributions are slightly slower than the experimentally determined  $P(E_T)$  distributions at both photon energies. A prior distribution was not calculated for channel 2

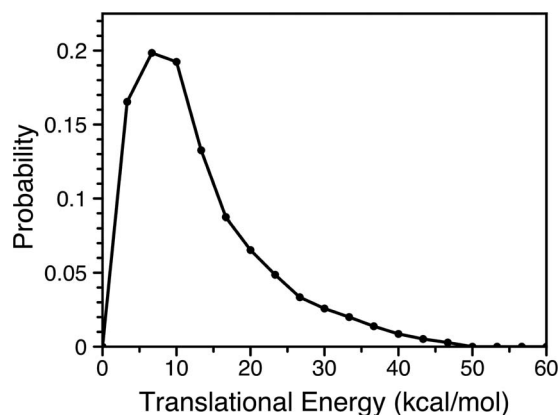


FIG. 9. Channel 2 translational energy distribution used to simultaneously simulate the  $m/z = 51$  and  $m/z = 26$  TOF spectra. Characteristics of this distribution are given in Table I.

as Eq. (6) is generally not applicable to reactions proceeding over a barrier.

The assignment of the two features observed in the TOF spectra at  $m/z = 50$  and  $\Theta_{\text{lab}} < 10^\circ$  to dissociative ionization of the  $m/z = 51$  and  $m/z = 76$  photofragments is supported by the agreement between the TOF data and the simulations for each channel as well as the dependence of the slower feature on  $\Theta_{\text{lab}}$ . Thus, these spectra can be used to calculate the product branching ratio. The channel 2/channel (1 + 3) branching ratio (BR) can be calculated using the following equation:

$$\text{BR} = R \times \frac{\sigma_{\text{C}_6\text{H}_4}}{\sigma_{\text{C}_4\text{H}_3}} \times \frac{f_{\text{C}_6\text{H}_4}}{f_{\text{C}_4\text{H}_3}}. \quad (7)$$

Here,  $R$  represents the ratio of contributions from each  $P(E_T)$  distribution used in the total TOF simulation. The second term, denoted by  $\sigma$ , is the relative ionization cross section for each photofragment and is estimated using the additive method of Fitch and Sauter.<sup>60</sup> The final variable in Eq. (7),  $f$ , is the fraction of the total photofragment signal for each channel that appears at  $m/z = 50$ . To determine the value of  $f$  for each channel, TOF spectra were taken at  $\Theta_{\text{lab}} = 7^\circ$  for all values of  $m/z$  that yield measurable signal ( $m/z = 76, 75, 74, 73, 61, 51, 50, 49, 37$ , and  $36$ ). The amount of signal from each channel was then determined for each mass-to-charge ratio: 40% of the total  $\text{C}_6\text{H}_4$  signal and 52% of the total  $\text{C}_4\text{H}_3$  signal appear at  $m/z = 50$ , compared to 11% and 10% at the parent ion masses of 76 and 51.

Using the  $P(E_T)$  distributions in Figures 8 and 9 for the N<sub>2</sub>/He gas mixture, Eq. (7) gives a channel 2/channel (1 + 3) branching ratio of 0.2, a BR in favor of the combined H-atom loss pathway. Similarly, using our published<sup>50</sup>  $f$  values in Eq. (7) and the pure He  $P(E_T)$  distribution in Fig. 8, simulations of TOF spectra for  $m/z = 50$  taken in He yield BR = 0.8. In order to estimate the error for each branching ratio, we calculated the parameter  $R$  in Eq. (7) over a range of  $P(E_T)$  distributions for H-atom loss that produced reasonable agreement with each set of  $m/z = 76$  TOF spectra. This procedure yields BR =  $0.2 \pm 0.1$  for N<sub>2</sub>/He and BR =  $0.8 \pm 0.2$  for pure He.

It thus appears that the branching ratio is remarkably and reproducibly sensitive to the carrier gas composition. There also appears to be a strong correlation between the form of the  $P(E_T)$  distribution for H-atom loss and the overall branching ratio. In simulating the N<sub>2</sub>/He data at  $m/z = 50$ , such as that in Fig. 4, the slower  $P(E_T)$  distribution for channels (1 + 3) relative to that in pure He necessitates increasing the contribution from H-atom loss (dotted line in Fig. 4) in order

to achieve satisfactory agreement between the overall simulation and the TOF spectra.

## V. DISCUSSION

The primary question of this investigation is whether the phenyl radical dissociation at 193 nm proceeds *via* internal conversion to the ground electronic state followed by statistical dissociation. The N<sub>2</sub>/He P( $E_T$ ) distributions for H-atom loss are only slightly faster than the prior distributions, consistent with statistical dissociation with no exit barrier. The corresponding distribution for channel 2 peaks further away from  $E_T = 0$ , as expected for dissociation over a small exit barrier as shown in Fig. 1. The branching ratio of  $0.2 \pm 0.1$  for channel 2/channels (1+3) is in reasonable agreement with the value of 0.17 from the RRKM calculations of Mebel and Landera.<sup>29</sup> This set of observations implies that the phenyl radical dissociates statistically on the ground state surface.

The branching ratio obtained using the N<sub>2</sub>/He mix, however, is considerably lower than that obtained here for pure He (0.8), and is in serious disagreement with our previous experimental result of 5.3 in favor of channel 2.<sup>50</sup> Moreover, the P( $E_T$ ) distributions for H-atom loss are considerably slower than those reported in our previous work at both 193 nm and 248 nm. To understand these differences, we examine the current results in detail and compare them to previous experimental and theoretical work.

The theoretical study by Mebel<sup>29</sup> showed that channels associated with ring-opening, *i.e.*, channels 2 and 3, become progressively more important as the available energy of the phenyl radical increases. Specifically, they found channel 2 to be the dominant channel when the available energy is equivalent to two-photon absorption at either 248 nm or 193 nm. Along the reaction coordinates for channels 2 and 3, the RRKM rate constant for ring opening increases by over four orders of magnitude as the internal energy is raised from 115.3 kcal/mol (one photon at 248 nm) to 296.3 kcal/mol (two-photon absorption at 193 nm), whereas the ring closure rate constant rises by less than a factor of three over the same energy range. This result reflects the fact that in the statistical limit, the electronic energy from photoexcitation is rapidly converted to internal energy on the ground state surface and that with increasing excitation energy the entropically favored—but higher energy—ring-opened dissociation channels become dominant. Essentially, once ring-opening occurs at high internal energy, ring-closure is highly unlikely.

In order to test whether the branching ratio reported by Negru *et al.*<sup>50</sup> resulted from two-photon excitation at 193 nm, we reduced<sup>56</sup> the laser fluence from 500 to <100 mJ/cm<sup>2</sup> using our original experimental conditions: high pressure pure He as the carrier gas.<sup>50</sup> Reducing the photon fluence had a negligible effect on the branching ratio and the shape of TOF spectral features, suggesting that two-photon excitation was unimportant in our original experiments.

However, the work by Mebel<sup>29</sup> and the calculated rate constants by Madden *et al.*<sup>28</sup> imply that channel 2 is also favored if the nascent internal energy  $E_0$  (see Eq. (5)) of the phenyl radical is raised. This consideration motivated our at-

tempts to produce colder phenyl radicals from our pyrolysis source by adjusting the composition of the carrier gas. Here, we found a significant effect. Using 10% N<sub>2</sub> in He resulted in slower P( $E_T$ ) distributions for H-atom loss at both photodissociation wavelengths and, at 193 nm, a branching ratio much closer to the H-atom loss dominant ratio predicted by Mebel's RRKM calculations. As shown in the SM, experiments with 10% Ar in He and 10% CO<sub>2</sub> in He carrier gas mixtures gave similar results.<sup>56</sup> When we reverted to a pure He carrier gas while holding all other experimental conditions constant, as shown in Fig. 5(a), the resulting TOF spectra at 193 nm could only be adequately simulated using the faster, pure He P( $E_T$ ) distribution in Fig. 8, and the branching ratio again showed channel 2 to be dominant (although not as dominant as seen previously<sup>50</sup>).

The choice of carrier gas is known to have an effect on the internal energy of a seeded molecule in a molecular beam (see, for example, Ref. 61). It thus appears that since N<sub>2</sub> is a heavier collider and has more degrees of freedom than He, the phenyl radicals are more effectively cooled by the N<sub>2</sub>/He carrier gas mixture than by pure He, thus lowering  $E_0$  and reducing the energy available to the photofragments. The lowered nascent internal energy results in a slower P( $E_T$ ) distribution for H-atom loss and, at 193 nm, contributes to a shift in branching ratio favoring H-atom loss over acetylene loss. Note that the P( $E_T$ ) distribution for channel 2 is largely unchanged, perhaps reflecting the presence of the exit barrier for this channel.

Based on the RRKM results of Mebel,<sup>29</sup> a BR  $\approx 1$  would result from a phenyl radical internal energy of  $\sim 180$  kcal/mol,  $\sim 30$  kcal/mol higher than a 193 nm photoexcited phenyl radical. The cooling of vibrationally excited benzyl radicals by collisions with N<sub>2</sub> is known to reduce the internal energy by 140 cm<sup>-1</sup> per collision.<sup>62</sup> A 30 kcal/mol decrease in  $E_0$  would thus require less than 100 collisions with N<sub>2</sub>. From our experimental parameters, we estimate the number of collisions during the expansion<sup>63</sup> to be several thousand, suggesting that this decrease in  $E_0$  due to the addition of 10% N<sub>2</sub> is reasonable.

The BR of  $0.8 \pm 0.2$  found here using pure He as the carrier gas is considerably lower than our previously reported value of 5.3.<sup>50</sup> Close examination of the original  $m/z = 50$  TOF spectra shows that simulations from the published H-atom loss P( $E_T$ ) distribution do not have sufficient intensity along the trailing edge of the observed feature. A slower H-atom loss distribution could account for this discrepancy and would also increase the contribution from this channel in the BR. However, the sensitivity of the BR to small differences in P( $E_T$ ) distributions was not appreciated at the time, and the overall simulations were thought to provide reasonable agreement with the data. Moreover, as discussed in Sec. II, the photodissociation of any remaining nitrosobenzene in the molecular beam yields signal in the  $m/z = 50$  TOF spectra that strongly overlaps the contribution from channel 2. Simulations of these spectra in which only phenyl dissociation is assumed would appear to require higher contribution from channel 2 to match the total signal, *i.e.*, a larger value for  $R$  in Eq. (7). It is thus possible that our previously published  $m/z = 50$  TOF spectra were contaminated in this way, resulting in

an additional contribution to erroneously high BR in favor of channel 2.

The  $P(E_T)$  distribution reported here for H-atom loss at 248 nm is slower than those measured by Song *et al.*<sup>52</sup> from 226 nm to 255 nm (245 nm is the closest point of comparison), whereas our earlier distribution<sup>50</sup> was somewhat faster. In their experiment, phenyl was produced by photolysis of chlorobenzene or bromobenzene seeded in Ar at a backing pressure of  $\sim 1.2$  atm. The UV photolysis of chlorobenzene is known to produce phenyl with substantial internal energy,<sup>17</sup> so it is possible that the discrepancies between this measurement and ours also reflect the extent of cooling by the carrier gas once the phenyl radicals are formed. Song *et al.* also observed a decrease in  $\langle f_T \rangle$  with increasing photon energy, consistent with our results at 248 and 193 nm.

## VI. CONCLUSIONS

We have re-evaluated the photodissociation of the phenyl radical, optimizing experimental conditions to cool the radicals and to reduce signal from any contaminants in the phenyl radical beam. This work is particularly concerned with the product branching ratio for the photodissociation of the phenyl radical at 193 nm and the implications that this ratio has for the photodissociation mechanism. We find that the branching ratio of acetylene loss to combined H-atom is 0.2, in agreement with the RRKM result of 0.17 (Ref. 29) and consistent with a statistical dissociation on the ground state surface. This value results from experiments in which the phenyl radical is formed in  $N_2$ /He carrier gas mixture; a considerably higher value of 0.8 is found when pure He is used as the carrier gas. In addition, the mixed carrier gas results in  $P(E_T)$  distributions for H-atom loss at 248 nm and 193 nm with decreased average translational energies. The dependence of the BR on  $P(E_T)$  distributions implies that the addition of  $N_2$  results in more effective cooling of the phenyl radicals after pyrolysis. While these results suggest that the previous work by Negru *et al.*<sup>50</sup> was also affected by excess internal energy in the phenyl radicals, the considerably higher branching ratio reported therein most likely reflects two additional effects: an overly fast  $P(E_T)$  distribution for H-atom loss and incomplete pyrolysis of the nitrosobenzene precursor in the radical source. The conclusions presented here represent a cautionary note when using flash pyrolysis sources to generate radicals and show that extra care must be taken to ensure contaminant-free production and sufficient cooling of the radical.

## ACKNOWLEDGMENTS

This work was supported by the Director, Office of Basic Energy Sciences, Chemical Sciences, Geosciences, and Biosciences Division of the U.S. Department of Energy under Contract No. DE-AC02-05CH11231.

<sup>1</sup>M. Frenklach, *Phys. Chem. Chem. Phys.* **4**, 2028 (2002).

<sup>2</sup>B. V. Unterreiner, M. Sierka, and R. Ahlrichs, *Phys. Chem. Chem. Phys.* **6**, 4377 (2004).

<sup>3</sup>B. Shukla, A. Susa, A. Miyoshi, and M. Koshi, *J. Phys. Chem. A* **112**, 2362 (2008).

<sup>4</sup>H. Richter and J. B. Howard, *Prog. Energy Combust. Sci.* **26**, 565 (2000).

- <sup>5</sup>J. A. Miller, M. J. Pilling, and J. Troe, *Proc. Combust. Inst.* **30**, 43 (2005).
- <sup>6</sup>B. S. Haynes and H. G. Wagner, *Prog. Energy Combust. Sci.* **7**, 229 (1981).
- <sup>7</sup>H. F. Calcote, *Combust. Flame* **42**, 215 (1981).
- <sup>8</sup>E. J. Highwood and R. P. Kinnersley, *Environ. Int.* **32**, 560 (2006).
- <sup>9</sup>M. Shiraiwa, K. Selzle, and U. Pöschl, *Free Radical Res.* **46**, 927 (2012).
- <sup>10</sup>R. I. Kaiser, L. Vereecken, J. Peeters, H. F. Bettinger, P. v. R. Schleyer, and H. F. Schaefer III, *Astron. Astrophys.* **406**, 385 (2003).
- <sup>11</sup>X. Gu and R. I. Kaiser, *Acc. Chem. Res.* **42**, 290 (2009).
- <sup>12</sup>D. S. N. Parker, F. Zhang, Y. S. Kim, R. I. Kaiser, A. Landera, V. V. Kislov, A. M. Mebel, and A. G. G. M. Tielens, *PNAS* **109**, 53 (2012).
- <sup>13</sup>N. Ikeda, N. Nakashima, and K. Yoshihara, *J. Am. Chem. Soc.* **107**, 3381 (1985).
- <sup>14</sup>J. G. Radziszewski, *Chem. Phys. Lett.* **301**, 565 (1999).
- <sup>15</sup>V. Butcher, M. L. Costa, J. M. Dyke, A. R. Ellis, and A. Morris, *Chem. Phys.* **115**, 261 (1987).
- <sup>16</sup>J. Hrušák, D. Schröder, and S. Iwata, *J. Chem. Phys.* **106**, 7541 (1997).
- <sup>17</sup>N. E. Sveum, S. J. Goncher, and D. M. Neumark, *Phys. Chem. Chem. Phys.* **8**, 592 (2006).
- <sup>18</sup>R. F. Gunion, M. K. Gilles, M. L. Polak, and W. C. Lineberger, *Int. J. Mass Spectrom. Ion Processes* **117**, 601 (1992).
- <sup>19</sup>G.-S. Kim, A. M. Mebel, and S. H. Lin, *Chem. Phys. Lett.* **361**, 421 (2002).
- <sup>20</sup>K. Freel, J. Park, M. C. Lin, and M. C. Heaven, *Chem. Phys. Lett.* **507**, 216 (2011).
- <sup>21</sup>G. T. Buckingham, C.-H. Chang, and D. J. Nesbitt, *J. Phys. Chem. A* **117**, 10047 (2013).
- <sup>22</sup>E. N. Sharp, M. A. Roberts, and D. J. Nesbitt, *Phys. Chem. Chem. Phys.* **10**, 6592 (2008).
- <sup>23</sup>J. C. Rienstra-Kiracofe, D. E. Graham, and H. F. Schaefer III, *Mol. Phys.* **94**, 767 (1998).
- <sup>24</sup>M. J. S. Dewar, W. C. Gardiner, Jr., M. Frenklach, and I. Oref, *J. Am. Chem. Soc.* **109**, 4456 (1987).
- <sup>25</sup>S. P. Walch, *J. Chem. Phys.* **103**, 8544 (1995).
- <sup>26</sup>J.-H. Huang, K.-L. Han, W.-Q. Deng, and G.-Z. He, *Chem. Phys. Lett.* **273**, 205 (1997).
- <sup>27</sup>X. Lories, J. Vandooren, and D. Peeters, *Phys. Chem. Chem. Phys.* **12**, 3762 (2010).
- <sup>28</sup>L. K. Madden, L. V. Moskaleva, S. Kristyan, and M. C. Lin, *J. Phys. Chem. A* **101**, 6790 (1997).
- <sup>29</sup>A. M. Mebel and A. Landera, *J. Chem. Phys.* **136**, 234305 (2012).
- <sup>30</sup>S. Olivella and A. Solé, *J. Am. Chem. Soc.* **122**, 11416 (2000).
- <sup>31</sup>H. Wang, A. Laskin, N. W. Moriarty, and M. Frenklach, *Proc. Combust. Inst.* **28**, 1545 (2000).
- <sup>32</sup>S. E. Wheeler, W. D. Allen, and H. F. Schaefer III, *J. Chem. Phys.* **121**, 8800 (2004).
- <sup>33</sup>S. J. Klippenstein and J. A. Miller, *J. Phys. Chem. A* **109**, 4285 (2005).
- <sup>34</sup>F. Zhang, D. Parker, Y. S. Kim, R. I. Kaiser, and A. M. Mebel, *Astrophys. J.* **728**, 141 (2011).
- <sup>35</sup>S. H. Bauer and C. F. Aten, *J. Chem. Phys.* **39**, 1253 (1963).
- <sup>36</sup>J. H. Kiefer, L. J. Mizerka, M. R. Patel, and H.-C. Wei, *J. Phys. Chem.* **89**, 2013 (1985).
- <sup>37</sup>M. Braun-Unkhoff, P. Frank, and T. Just, *Proc. Combust. Inst.* **22**, 1053 (1988).
- <sup>38</sup>A. Laskin and A. Lifshitz, *Proc. Combust. Inst.* **26**, 669 (1996).
- <sup>39</sup>J. C. Scaiano and L. C. Stewart, *J. Am. Chem. Soc.* **105**, 3609 (1983).
- <sup>40</sup>A. Mardyukov, R. Crespo-Otero, E. Sanchez-Garcia, and W. Sander, *Chem. Eur. J.* **16**, 8679 (2010).
- <sup>41</sup>T. Yu and M. C. Lin, *J. Phys. Chem.* **99**, 8599 (1995).
- <sup>42</sup>I. V. Tokmakov, J. Park, and M. C. Lin, *ChemPhysChem* **6**, 2075 (2005).
- <sup>43</sup>J. Park, G. J. Nam, I. V. Tokmakov, and M. C. Lin, *J. Phys. Chem. A* **110**, 8729 (2006).
- <sup>44</sup>A. Yokoyama, X. Zhao, E. J. Hints, R. E. Continetti, and Y. T. Lee, *J. Chem. Phys.* **92**, 4222 (1990).
- <sup>45</sup>C.-M. Tseng, Y. M. Choi, C.-L. Huang, C.-K. Ni, Y. T. Lee, and M. C. Lin, *J. Phys. Chem. A* **108**, 7928 (2004).
- <sup>46</sup>D. R. Albert, M. A. Todt, and H. F. Davis, *J. Phys. Chem. A* **117**, 13967 (2013).
- <sup>47</sup>F. Zhang, B. Jones, P. Maksyutenko, R. I. Kaiser, C. Chin, V. V. Kislov, and A. M. Mebel, *J. Am. Chem. Soc.* **132**, 2672 (2010).
- <sup>48</sup>D. S. N. Parker, F. Zhang, and R. I. Kaiser, *J. Phys. Chem. A* **115**, 11515 (2011).
- <sup>49</sup>D. S. N. Parker, F. Zhang, R. I. Kaiser, V. V. Kislov, and A. M. Mebel, *Chem. Asian J.* **6**, 3035 (2011).
- <sup>50</sup>B. Negru, S. J. Goncher, A. L. Brunsvold, G. M. P. Just, D. Park, and D. M. Neumark, *J. Chem. Phys.* **133**, 074302 (2010).

- <sup>51</sup>D. W. Kohn, H. Clauberg, and P. Chen, *Rev. Sci. Instrum.* **63**, 4003 (1992).
- <sup>52</sup>Y. Song, M. Lucas, M. Alcaraz, J. Zhang, and C. Brazier, *J. Chem. Phys.* **136**, 044308 (2012).
- <sup>53</sup>Y. T. Lee, J. D. McDonald, P. R. LeBreton, and D. R. Herschbach, *Rev. Sci. Instrum.* **40**, 1402 (1969).
- <sup>54</sup>J. C. Robinson, S. A. Harris, W. Sun, N. E. Sveum, and D. M. Neumark, *J. Am. Chem. Soc.* **124**, 10211 (2002).
- <sup>55</sup>B. Negru, G. M. P. Just, D. Park, and D. M. Neumark, *Phys. Chem. Chem. Phys.* **13**, 8180 (2011).
- <sup>56</sup>See supplementary material at <http://dx.doi.org/10.1063/1.4894398> for details concerning experimental conditions, possible contaminants, and biphenyl photodissociation.
- <sup>57</sup>N. R. Daly, *Rev. Sci. Instrum.* **31**, 264 (1960).
- <sup>58</sup>S. A. Harich, PHOTRAN, a program for forward convolution analysis of photodissociation, 2003.
- <sup>59</sup>T. Baer and W. L. Hase, *Unimolecular Reaction Dynamics: Theory and Experiments* (Oxford University Press, 1996).
- <sup>60</sup>W. L. Fitch and A. D. Sauter, *Anal. Chem.* **55**, 832 (1983).
- <sup>61</sup>D. E. Powers, J. B. Hopkins, and R. E. Smalley, *J. Phys. Chem.* **85**, 2711 (1981).
- <sup>62</sup>M. Damm, F. Deckert, and H. Hippler, *Ber. Bunsenges. Phys. Chem.* **101**, 1901 (1997).
- <sup>63</sup>G. Scoles, *Atomic and Molecular Beam Methods: Volume I* (Oxford University Press, 1988).